Original Research Article

First-principles Investigation of Structure and electronic properties of $NiTe_2$ Fermi Crossing Type-II Dirac Semimetal.

[*]Muzambilu Saminu[1], Sofwan Ibrahim Saleh[1], Shafiu Ibrahim Musa[1],Gulzar Ahmed[1], M. C. Idris[2]
[1]Physics Department, Mewar University, Chittorgarh, Rajasthan, India.
[2]Physics Department, Sule Lamido University, Kafin Hausa, Jigawa State, Nigeria.

ABSTRACT
The electronic structure aspect of transition metal dichalcogenides (TMDs) has so far received intensive research interest. $NiTe_2$ is a noble candidate for type-II DSM with Dirac point near the Fermi surface. In this paper we present a systematic investigation of the structural stabilities and electronic properties of $NiTe_2$ using density functional theory via a plane wave pseudopotentialmethod in the context of the Perdew–Burke–Ernzerhof generalized gradient approximation. The structural parameters, partial and total density of states (DOS) were systematically studied. Our structural study indicates that the material has a trigonal structure with $P\bar{3}m_1$ space group. In addition, wehave computed the cohesive energy and the DOS at the Fermi level [$N(E_f)$]. The results show that $NiTe_2$ is stable.
Keywords: DFT, Structural properties, Dirac semimetal, $NiTe_2$, Dichalcogenides

1. INTRODUCTION
The combination of nickel and telluride in the Ni-chalcogenides family are the very few being perceived due to the nature of tellurium that is comparatively denser than both Selenium and Sulphur, thus poorly adhesive onto the substrate [1]. Nguyen et al. studied the structure of liquid $NiTe_2$ by using the technique of neutron diffraction [2]. Lately, 2D materials have captured a great deal of study focused particularly because of their separate physical properties and ability to fulfill the future demands of the nano-electronic industry on adaptability, multi-functionality, and flexibility. During investigating for expected promising materials, layered transition metal di-chalcogenides have been important members of the 2D materials [3]

Immediately after the discovery of 3D Dirac semimetals (DSMs), which are regarded as type-II fermions in which the Dirac node is enclosed by an electron pocket, has generated a huge research interest because of the rich physics involve and the tremendous applications therein. Recently the attention has been shifted partially to the so-called type-II Dirac semimetals where the Dirac cone is strongly tilted because of the broken Lorentz symmetry, and due to that, the Dirac point appears only at the contact of hole and electron pockets [4-5]. Transition metal di-chalcogenides offer a perfect platform to experimentally understand Dirac fermions. Though, usually, these interesting quasiparticles are situated far-away from the Fermi level, restraining the contribution of Dirac-like carriers to the transport properties. $NiTe_2$ accommodates both bulk Type-II Dirac points and topological surface states [6]. Type-II Dirac semimetals also called Weyl semimetals are characterized by strongly tilted Dirac cones in a way that Dirac the Dirac node emerges at the boundary of electron and hole pockets as a new state of Quantum matter, different from the standard Weyl points with a point like Fermi surface which is called as type-I nodes. The type-II Dirac semimetals were recently predicted by theory and have since been confirmed experimentally in some other transition metal di-chalcogenides [7]. Even recently, many transition metal di-chalcogenide materials, comprising of $PtTe_2$, $PdTe_2$, and $PtSe_2$, were predicted and found to display tilted Dirac cones close to their Fermi surface. For these considered Dirac type-II compounds, the Hamiltonian comprises of the type-I linear Hamiltonian and an additional, momentum dependent, a term

that breaks Lorentz invariance and leads to quasiparticles showing a momentum energy relation that depends on the direction of travel [8]. New quantum phenomena like the planar Hall effect and superconductivity have been theoretically projected and experimentally confirmed in bulk $NiTe_2$ [9]. Most of the transition metal di-chalcogenides can achieve superconductivity by pressure or doping. Investigation on the pressure-resistant impression on resistant behavior of $NiTe_2$. $NiTe_2$ shows the metallic property at ambient pressure in temperature ranging from 2000-3000000^{O}C [10].

Recent studies on $NiTe_2$ proposed to find experimental evidence for its existence through the mapping of its electronic band structure via angle-resolved-photoemission spectroscopy (ARPES) measurement or extracting its Berry phase from magnetization measurements [11-12]. Though some information about the Fermi surface topography, extracted from the angular dependence of the quantum oscillations, along with a comparison with density functional theory calculations were reported detailed information on structural properties of $NiTe_2$ is still debatable. Therefore, in this paper, we investigated the detailed structural stabilities and electronic properties of $NiTe_2$ as a Fermi crossing Dirac type-II semimetal candidate.

2.COMPUTATIONAL DETAILS

Theoretically,the Schrodinger Equation (SE) is a quantum mechanical idea that provides the exact manners and behavior of a system's natural states like particle motion and its wave-function. The electronic structure of any system can be accurately obtained using the solution of SE without any empirical or semi-empirical parameters [13-14]. Though the SE is not easy to solve because of the nucleus-electron interaction, thereafter a solution was suggested by prominent Born-Oppenheimer approximation. Earlier scholars assume that to split electronic coordinates and nuclear from many-body wave function, the nuclei must be assessed adiabatically because of the variation in mass between electron and nuclei [15]. Even though with this clarification and simplification yet, the many-body problem remains enormously problematic to work out. Then via the Hartree-Fock (H-F) approximation, many body-problems can be simplified to a single-electron problem and offer an exact description of electron exchange, sadly it did not describe the electronic correlation [16]. Because, it is not possible to solve the SE for N-electron, in the year 1964 density functional theory (DFT) was introduced by the renowned Hohenberg and Kohn as a technique to offers the description of the electronic structure of a system at ground state with the idea stated that all ground sate properties for many-systems are functional of the ground state density [17-18]. The minimum value of the total energy functional is the definite single electron ground state density [19]. Kohn and Sham suggested an equation that succeeded in replacing the problem of mutually interacting electrons in an external ion potential to an equivalent set of self-consistent one electron [20]. The significance of electron-electron interaction is provided by Generalized Gradient Approximation (GGA) [21]. Computations based on density functional theory are well-known and distinguished from other ab initio methods as first principle calculations with an approximate error of 10^{-3} eV, the errors can be significantly minimized by adjusting the K-points mesh or the cutoff energy. In numerous cases, the first-principles calculations within the density functional theory framework offer exact guesses of many properties of materials, stable configuration, and total energy.

In this work, we perform the first-principles calculations using the Plane-Wave Self-consistent field (PWSCF) program of the Quantum ESPRESSO simulation code [23] based on the density functional theory (DFT). The cut-off energy for the wavefunction is taken to be 150 Ry. K-point grid in the Brillouin

zone is set to be 8 × 8 × 1 grid for $NiTe_2$ in the Monkhorst-Pack method. [24]. The Generalized Gradient Approximation (GGA) of Perdew-Burke-Ernzerhof (PBE) formalism is adopted for the exchange-correlation (XC) functional [25] and is used for computing the electronic properties of the material. To obtain optimized atomic configurations of $NiTe_2$, variable cell relaxations for atomic coordinates and dimension of the cell using intrinsic Broyden-Fletcher-Gold farb-Shanno (BFGS) algorithm were performed. Fig. 1(a) and 1(b) display the first Brillouin zone and the relax structure of $NiTe_2$. The model is considered as an optimized structure when the Hellmann-Feynman forces and all components of the stress are less than 0.0005 Ry/a.u respectively.

3. RESULTS AND DISCUSSION

3.1 Structural Parameters

The complete relaxation calculations were initially performed to determine the accurate internal positions of the atoms. All atomic positions and lattice parameters were optimized. The numerical calculation was implemented in the Quantum ESPRESSO simulation package. The calculated lattice parameters, Fermi energy, density, and volume for the relaxed structure of $NiTe_2$ are given in Table 1 below. It is worth noting that the result of our calculations is in good agreement with experimental data. Ni and Te consist of stacked Te-Ni-Te layers, where the metal Ni atom is coordinated octahedrally with six atoms of Te. The atoms are covalently bonded within one layer, while the sandwich layers are coupled only by weak Vander Waals interaction [26]. Fig. 1 depicts the total energy against the volume of $NiTe_2$. The optimized lattice parameters of $NiTe_2$ a_o(3.8032), b_o(3.8032), c_o(5.9506) via GGA-PBE are in good agreement with other theoretical and experimental values. The discrepancy of lattice parameters is within 0.105% when compared with the experimental value. The maximum error of c_o(5.9506) using GGA-PBE reaches about 3.1%. the lattice parameters a_o of $NiTe_2$ is about 0.05 Å lower than other theoretical calculations.

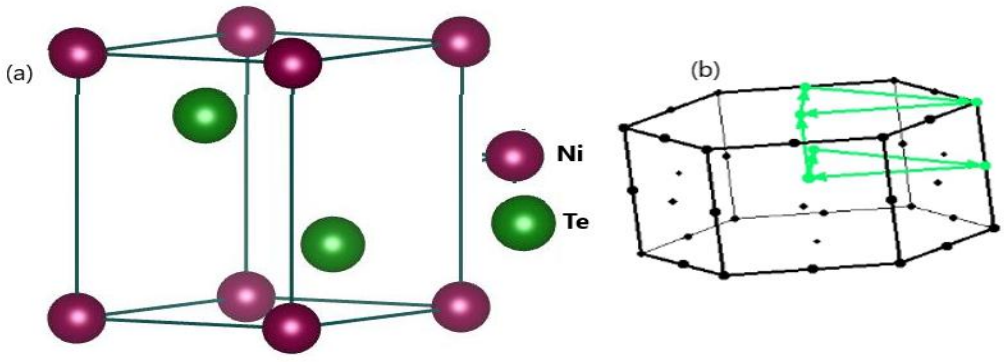

Fig. 1. (a) VESTA view of $NiTe_2$ and (b): first Brillouin zone of $NiTe_2$ from XCRYSDEN

Table 1. Calculated equilibrium lattice parameter, volume, density, minimum energy E_0, and the enthalpy of formation of $NiTe_2$

	a = b (Å)	c(Å)	V $(Å)^3$	ρ (g/cm^3)	E_0 (Ry)	H (Ry)	B(Gpa)	B’

This work	3.7925	5.9395	73.98365	7.01381	-157.58461	-396.22229	224.6	1.00
Experiment [28]	3.899	5.243	69.036	7.550				

Also using the Birch-Murnaghan equation of state (EOS) given by Equation (1). The optimization of the relaxed structure of $NiTe_2$ was carried out by GGA-PBE to compute the ground state properties which consist of the bulk modulus B_o and the first derivative of the modulus B' [27].

$$E(v) = E_o + \left\{ \left[\left(\frac{V_o}{V} \right)^{\frac{2}{3}} - 1 \right]^2 \left[(6-4) \left(\frac{V_o}{V} \right)^{\frac{2}{3}} \right] + \left[\left(\frac{V_o}{V} \right)^{\frac{2}{3}} - 1 \right]^3 B' \right\} \left(\frac{9 V_o B_o}{16} \right) \quad (1)$$

Where E_o and V_o are the minimum equilibrium energy and volume respectively. Fig. 2 depicts the optimization plot using GGA. For GGA we found that the lowest equilibrium energy value is -157.6 Ry corresponding to 500.4 $(a.u)^3$.

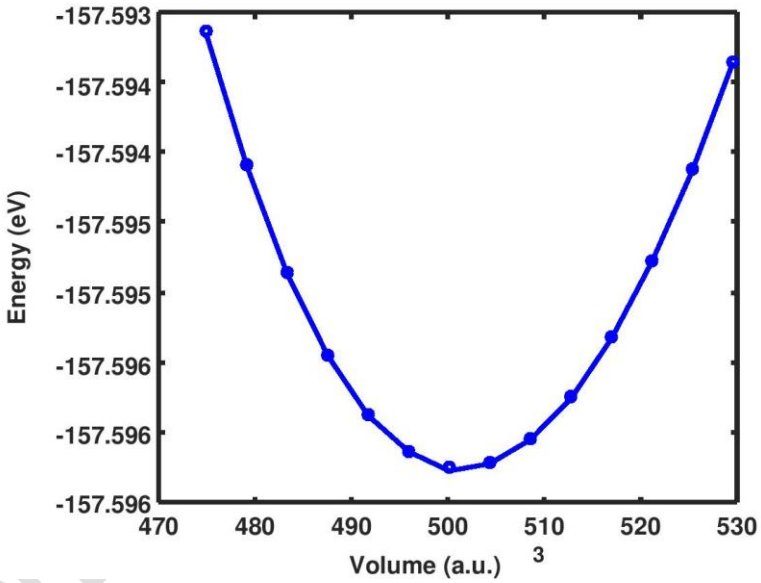

Fig. 2. Calculated total energy and volume of $NiTe_2$ using GGA

To show the thermodynamic stability of our material we calculated the enthalpy of formation H using the following Equation (2)

$$H = \frac{(E_T(NiTe_2) - mE_{Ni} - gE_{Te})}{(m+g)} \quad (2)$$

Where the term $E_T(NiTe_2)$ is the total ground state energy of the material been studied E_{Ni} and E_{Te} are the ground state energies of the Ni and Te in the unit cell respectively. The parameters m and g in the equation represent the number of the individual atoms in the unit cell. In this work, we reformed Equation (2) above for application on $NiTe_2$ Fermi Dirac type-II material for GGA-PBE as shown below.

$$H = \frac{E_T^{GGA}(NiTe2) - (mE_{Ni}^{GGA} - gE_{Te}^{GGA})}{(m+g)} \quad (3)$$

For a material to be stable, its total energy must be lower than the sum of energies of its components [29]. Consequently, the negative value obtained for the enthalpy of formation as presented in Table 1 confirms that the studied material is stable.

Cohesive energy is the work that is required when a solid is decomposed into a free isolated atom, the more negative the cohesive energy, the more stable the material, the expression of the cohesive energy is given in the equation below

$$E_{coh}^{NiTe_2} = \frac{E_{solid}^{NiTe_2} - Z \times (aE_{atom}^{Ni} + bE_{atom}^{Te_2})}{Z \times (a+b)} \quad (2)$$

where Z is the number of $NiTe_2$ per unit cell. To get the structural parameters, such as the equilibrium lattice parameters a, c, the bulk modulus B_o and its pressure first derivative B', we have computed the cohesive energy in Equation for $NiTe_2$. The cohesive energy as a function of the volume is fitted with Birch Murnaghan's first equation of state (EOS). The obtained cohesive energy against the volume data for $NiTe_2$ is shown graphically in Figure 2.

3.2 Electronic Properties

Figure 3 is the electronic band structure of $NiTe_2$. Dirac type-II is observed along with Gamma to H symmetry points direction with the node located above the Fermi level (E_f). The valence bands cross E_f. It is clear that Fermi level exists an electronic distribution, show that $NiTe_2$ has metallic properties. Within the Fermi level, the value of the density of states is 1.827 electrons/eV. The band structure of the semi-metals isclassified by a slight overlap between its valence and conduction band. It is from the perspective of the valence band to cross the conduction band to illustrate the appearance of free electrons is active at Ni-3d orbital. Therefore, $NiTe_2$ possesses the features of metallicity, indicating that $NiTe_2$ is semi-metal. The most important characteristic of a type-II Dirac semimetal is the tilted 3D Dirac cone in the band structure. Electronic band structure calculation is very important for describing the behavior of type-II Dirac materials. From our band structure calculations, the Fermi level lies at 0 eV and the valence band was found to lie above the Fermi level with Dirac cone pointing toward the Fermi level, hence the material is said to behave as Dirac type-II semimetal.

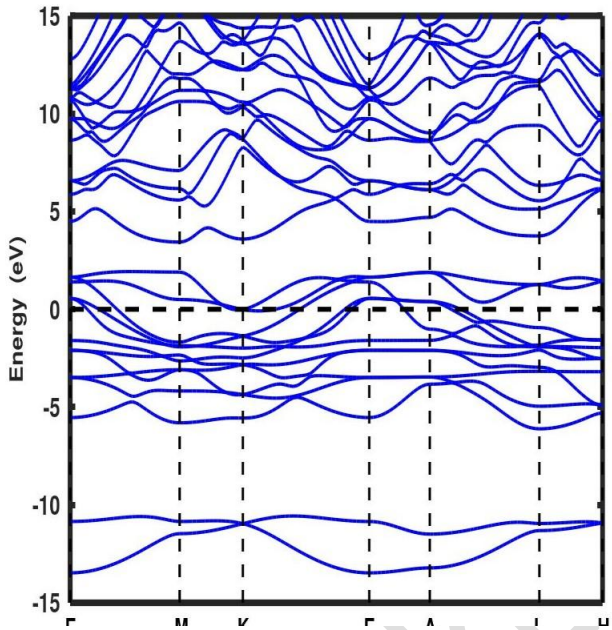

Fig. 3. Computed electronic band structure of $NiTe_2$ using GGA

We have also calculated and analyzed the total density of states (TDOS) and partial density of states (PDOS) for $NiTe_2$ as can be seen in Fig. 4 along with the fermi energy level represented by a pink dash. DOS aid the elaboration of the nature of the bandgap and PDOS provides detailed information about the origin of bands for both valence and conduction bands. In the total density of states plot, near the fermi level i.e at 0 eV there are available states which also shows that the studied material is behaving as a Dirac type-II semimetal. The TDOS confirms that the bands near the Fermi level, E_f, are dominated by Te p-orbital. Ni d-orbital derived bands appear away from the Fermi level.

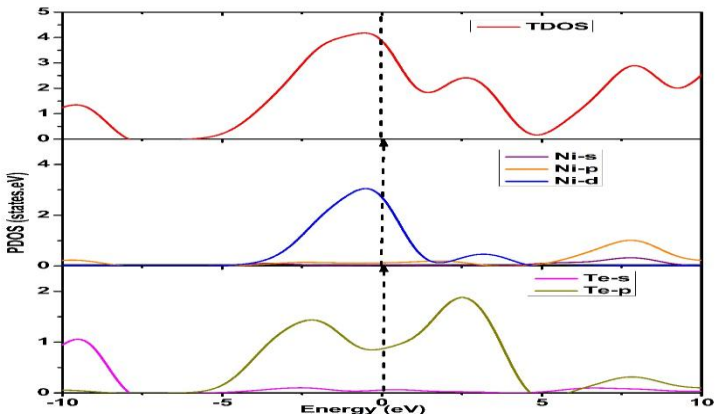

Fig. 4. the total density of states (TDOS) for $NiTe_2$ and the contribution of each of the individual orbitals of Ni and Te. Ni d-orbital contributed significantly in the conduction band and the p-orbital contributed also significantly in the valence band. While the p-orbital of Te contributed more in both the valence and conduction bands.

The total density and partial density of states (TDOS and PDOS) of $NiTe_2$ at 0 GPa are studied and displayed in Fig.3 the horizontal dashed line in the figure is the Fermi level (E_f). The density of states for $NiTe_2$ can be divided into three regions. For energy regions from -17.5eV to -10.00eV in this region the DOS is mainly composed of Te-s orbital; from -10.00eV in this region, the DOS to 4.00eV there is a hybridization between Te-d, Te-p orbitals and the Ni-d and Ni-p orbitals. Finally, within the energy region higher than 4.00eV Ni-p orbital and Te-p orbital constituted the DOS respectively

4. CONCLUSION

Structural and electronic properties of $NiTe_2$ are studied and analyzed by the first-principles calculations. Excellent agreement is found with other theoretical and experimental studies. According to the DOS, there is a constant electron distribution at the Fermi surface, which revealed that $NiTe_2$ is a Dirac type-II semi-metal. We predict that $NiTe_2$ is a noble candidate for type-II DSM. Our work establishes $NiTe_2$ as a major candidate for exploration of Dirac Fermions and applications in transition metal dichalcogenides based infrared plasmonics, spintronic devices, and ultrafast optoelectronics.

COMPETING INTERESTS

Authors have declared that no competing interests exist.

References

1. Anand, T.J.S.; Zaidan, M., Azam, M.A. et al. Structural studies of NiTe2 thin films with the influence of amino additives. Int J Mech Mater Eng 9, 18 (2014).
2. V T Nguyen1, M Gay1, J E Enderby1, R J Newport1, and R A Howie. The structure and electrical properties of liquid semiconductors.
3. Qianwen, W.; Peng, W.; Gengyu, C.; Min, H. First Principle Study of the Structural and Electronic Properties of MoS2-MoTe2 Monolayer Heterostructures. J. Phys. D: Appl. Phys. 46 (2013) 505308 (7pp).
4. Burkov, A. A. Topological Semi-metals. Nat. Mater. 2016,15, 1145-1148.
5. Soluyanov, A. A.; Gresch, D.; Wang, Z.; Wu, Q.; Troyer, M.; Dai, X.; Bernevig, B. A. Type-II Weyl Se-metals. Nature 2015, 527, 495-498.
6. Saumya, M.; Sophie, F.; Pabitra, K.; Timur, K.; Laurent, C.; Mathew, D.; Jeffrey, B. Fermi-crossing Type-II Dirac Fermions and Topological surface states in NiTe2. Scientific Reports, 2020, 10, 12957.
7. Chungian, X.; Bin, L.; Wen, J.; Wei, Z.; Bin, Q.; Raman, S.; Nikolai, D.; Zhigalo, Yanpeng, Q.; Fang-Cheng, C.; Xiaofeng, X. Topological Type-II Dirac Fermions Approaching the Fermi Level in a Transition Metal Dichalcogenide NiTe2. Chem. Mater. 2018, 14, 4823-4830
8. Huang, H.; Zhou, S.; Duan, W. Phys. Rev. B 94, 121117®, 2016.
9. Zheng, F. P.; Li, X.-B.; Tan, P.; Lin, Y. P.; Xiong, L. X.; Chen, X. B.; Feng, J. Emergent Superconductivity in Two Dimensional NiTe2 Crystals. Phys. Rev. B 2020, 101, 100505(R).
10. Tao, L.; Ke, W.; Chungiang, X.; Qian, H.; Hao, W.; Jun-Yi, G.; Shixun, C.; Jiang, Z.; Wei, R.; Xiaonfeng, X.; Nai-chang, Y.; Bin, C.; Zhenjie, F. Pressure-Induced Superconductivity in topological type-II Dirac semimetal NiTe2. Cond-Mat. Supr-Con. 2019.
11. Ghosh, B.; Mondal, D.; Kuo, C. N.; Lue, C. S.; Nayak, J.; Fujii, J.; Vobomik, I.; Politano, A.; Agarwala, A. Phys. Rev. B 100, 2019, 195134.

12. Xu, C.; Li, B.; Jiao, W.; Zhou, W.; Qian, B.; Sankar, R.; Zhigalo, N. D.; Qi, Y.; Qian, D.; Chou, F. C.; Xu, X. Chem. Mater. 30, 2018, 4823.

13. Foresman J, Frisch A. Exploring Chemistry with Electronic Structure Methods 2nded. Gaussian, Inc, Pittsburgh, PA.

14. Novak P, Boucher F, Gressier P, Blaha P, Schwarz K. Phys. Rev. B 63 (2001) 235114-1–8.

15. Filippov A, Non-linear Non-local Schrodinger equation in the contest of quantum mechanics. Phys. Lett A 1996; 215:32-9.

16. Callaway J, March N. Density Functional Methods: theory and application solid-state physics. 1984; 38:135-221.

17. Kuznetsov A, Medvedev I. Does Born-Oppenheimer Approximation Break Down in Charge Transfer Process? An Exactly Solvable Model. Chem. Phys. 2006; 324:148-59.

18. Chaikin P, Lubensky T. principles of Condensed Matter Physics. Cambridge Univ. Press; 2000.

19. Hohenberg P, Kohn W. Density Functional Theory. Phys. Rev. B 194; 136:864-76.

20. Dreizler R, Gross E. Density Functional Theory: An Approach to the Quantum Many-Body Problem. Springer Science & Business Media; 2012.

21. Payne M, Teter M, Allan D, Arias T, Joannopoulos J. Iterative Minimization Techniques for Ab Initio Total Energy Calculations Molecular Dynamics and Conjugate Gradients. Rev. Modern Phys. 1992; 64:1045.

22. Kohn W, Sham LJ. Self-Consistent Equations Including Exchange and Correlation Effects. Phys. Rev. 1965; 140:A1133.

23. Giannozzi, P.; Baroni, S.; Bonini, N.; Calandra, R.; Cavazzoni, C.; Caresoli, D.; Chiarotti, G.L.; Cococcioni, M.; Dabo, I. Jorn. Phys. Condens. Matter 21, 2009, 395502.
24. Monkhorst, H. J.; Pack, J. D. special points for Brillouin zone integrations. Phys. Rev. B 13, 12, 1976, 5188.
25. Perdew, J. P.; Burke, K.; Ernzerhof, M. Phys. Rev. Lett. 1996, 77, 3865-3868.
26. Hartwigsen, S. Goedecker, J. Hutter, Relativistic separable dual-space Gaussian pseudopotentials from H to Rn, Phys. Rev. B 58,1998, 3641.
27. Birch, F. Finite elastic strain of cubic crystal. Phys. Rev. 71. 1947. 809-824.
28. Jain, A.; Ong S. P.; Hautier, G.; Chen, W.; Richards, W. D.; Deck, S.; Cholia, S.; Gunter, D.; Skinner, D.; Ceder, G.; Pearson, K. A. The Materials Project: A material genome approach to accelerating materials innovation APL Materials, 2013, 1(1), 011002.
29. Wu, S.; Fecher, G. H.; Shabab, S.; Felser, C. Elastic properties and stability of Heusler Compounds: cubic Co 2 YZ compounds with L 2 1 structure. J. Appl. Phys. 125 (2019).
30. Kudo, K.; Ishii, H.; Nohara, M. Composition-Induced Structural Instability and Strong-coupling Superconductivity In Au1-xPdxTe2 Phys. Rev. B 93 140505.